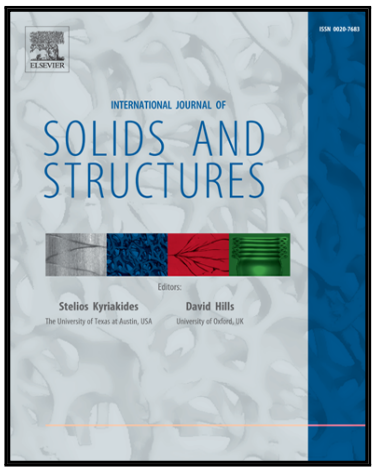

Non-prismatic Beams: a Simple and Effective Timoshenko-like Model

Giuseppe Balduzzi, Mehdi Aminbaghai, Elio Sacco, Josef Füssl, Josef Eberhardsteiner, Ferdinando Auricchio

PII: S0020-7683(16)00079-2
DOI: 10.1016/j.ijsolstr.2016.02.017
Reference: SAS 9062

To appear in: *International Journal of Solids and Structures*

Received date: 3 July 2015
Revised date: 2 February 2016
Accepted date: 10 February 2016

Please cite this article as: Giuseppe Balduzzi, Mehdi Aminbaghai, Elio Sacco, Josef Füssl, Josef Eberhardsteiner, Ferdinando Auricchio, Non-prismatic Beams: a Simple and Effective Timoshenko-like Model, *International Journal of Solids and Structures* (2016), doi: 10.1016/j.ijsolstr.2016.02.017

Non-prismatic Beams: a Simple and Effective Timoshenko-like Model

Giuseppe Balduzzi[a,*], Mehdi Aminbaghai[b], Elio Sacco[c], Josef Füssl[b], Josef Eberhardsteiner[b], Ferdinando Auricchio[a]

[a] *Department of Civil Engineering and Architeture (DICAr), University of Pavia, Pavia, Italy*
[b] *Institute for Mechanics of Materials and Structures (IMWS), Vienna University of Technology, Vienna, Austria*
[c] *Department of Civil and Mechanical Engineering, University of Cassino and Southern Lazio, Cassino, Italy*

Abstract

The present paper discusses simple compatibility, equilibrium, and constitutive equations for a non-prismatic planar beam. Specifically, the proposed model is based on standard Timoshenko kinematics (i.e., planar cross-section remain planar in consequence of a deformation, but can rotate with respect to the beam center-line). An initial discussion of a 2D elastic problem highlights that the boundary equilibrium deeply influences the cross-section stress distribution, and all unknown fields are represented with respect to global Cartesian coordinates. A the simple beam model (i.e. a set of Ordinary Differential Equations (ODEs)) is derived, describing accurately the effects of non-prismatic geometry on the beam behavior and motivating equation's terms with both physical and mathematical arguments. Finally, several analytical and numerical solutions are compared with results existing in literature. The main conclusions can be summarized as follows. (i) The stress distribution within the cross-section is not trivial as in prismatic beams, in particular the shear stress distribution depends on all generalized stresses and on the beam geometry. (ii) The derivation of simplified constitutive relations highlights a strong dependence of each generalized deformation on all the generalized stresses. (iii) Axial and shear-bending problems are strictly coupled. (iv) The beam model is naturally expressed as an explicit system of six first order ODEs. (v) The ODEs solution can be obtained through the iterative integration of the right hand side term of each equation. (vi) The proposed simple model predicts the real behavior of non-prismatic beams with a good accuracy, reasonable for the most of practical applications.

Keywords: Non-prismatic Timoshenko beam, beam modeling, analytical solution, tapered beam, arches

*Corresponding author. *Adress*: Dipartimento di Ingengeria Civile e Architettura (DICAr), Università degli Studi di Pavia, via Ferrata 3, 27100 Pavia Italy *Email adress*: giuseppe.balduzzi@unipv.it *Phone*: 0039 0382 985 468

Email addresses: giuseppe.balduzzi@unipv.it (Giuseppe Balduzzi), mehdi.aminbaghai@tuwien.ac.at (Mehdi Aminbaghai), sacco@unicas.it (Elio Sacco), Josef.Fuessl@tuwien.ac.at (Josef Füssl), josef.eberhardsteiner@tuwien.ac.at (Josef Eberhardsteiner), ferdinando.auricchio@unipv.it (Ferdinando Auricchio)

1. Introduction

Non-prismatic beams –sometime mentioned also as *beams with non-constant cross-section* or *beams of variable cross-section*– are a particular class of slender bodies, object of the practitioners interest due to the possibility of optimizing their geometry with respect to specific needs (Timoshenko and Young, 1965; Auricchio et al., 2015). Despite the advantages that engineers can obtain from their use, non-trivial difficulties occurring in the non-prismatic beam modeling often lead to inaccurate predictions that vanish the gain of the optimization process (Hodges et al., 2010). As a consequence, an effective non-prismatic beam modeling still represents a branch of the structural mechanics where significant improvements are required.

Within the large class of non-prismatic beams it is possible to recognize several families of beams characterized by peculiar properties and intrinsic modeling problems. Unfortunately, the literature lexicon is not thorough and the language ambiguities could lead to some annoying misunderstanding. Therefore, in order to discuss the existing approaches, we introduce some terminology that we are going to use in this document.

- A *prismatic beam* is a prismatic slender body with straight center-line and constant cross-section.
- A *curved beam* is a body with a curvilinear center-line and constant cross-section (orthogonal to the center-line).
- A *beam of variable cross-section* is a beam with straight center-line and non-constant cross-section; sometime authors refer to this kind of bodies with the expression "non-prismatic beams" (Shooshtari and Khajavi, 2010; Attarnejad et al., 2010; Beltempo et al., 2015).
- A *tapered beam* is a beam of variable cross-section with the additional property that the cross-section size varies linearly with respect to the axis coordinate; sometime authors refer to this kind of bodies with the expression "beam of variable cross-section" (Cicala, 1939; Romano, 1996; Franciosi and Mecca, 1998; Sapountzakis and Panagos, 2008).
- A *twisted beam* is a beam of variable cross-section with the additional property that the cross-section rotation around the axis coordinate varies.
- A *non-prismatic beam* is the most general case we can consider, i.e. a beam with curvilinear center-line and non-constant cross-section.

Classical reference books treat separately curved beams and beams of variable cross-section, but do not provide any specific indications for the non-prismatic beams (Timoshenko, 1955; Timoshenko and Young, 1965). This distinction is substantially confirmed also in more recent books (Bruhns, 2003; Gross et al., 2012) and papers. As an example, Hodges et al. (2008, 2010) propose a model for a tapered beam whereas Rajagopal et al. (2012); Yu et al. (2002) focus on curvilinear beams.

Focusing on curvilinear beams, the classical approach describes the beam geometry through a curvilinear coordinate that runs along the beam center-line (Capurso, 1971; Bruhns, 2003). As a consequence, the cross-sections are defined as the intersection between the beam body and the plane orthogonal to the center-line at a fixed curvilinear coordinate. Furthermore, the resulting forces –ensuring the beam equilibrium– are expressed as function of a local coordinate system with the axes tangential, normal, and binormal to the center-line, respectively. For planar beams, the so far introduced choices lead to express the equilibrium through a system of 3 ODEs that are coupled and use non-linear coefficients (Rajasekaran and Padmanabhan, 1989; Arunakirinathar and Reddy, 1992, 1993; Yu et al., 2002; Rajagopal et al., 2012). The immediate consequence of this approach is that analytical solutions are available only for simple geometries, typically beams with constant curvature. An alternative approach was proposed by Gimena et al. (2008a) that express both displacements and resulting forces in a global coordinate system. The main advantage of the proposed approach is the simplicity of the resulting ODEs that could be solved with successive integrations.

Focusing on beams of variable cross-section, the literature presents a number of possible models that can be classified as follows:

- simple models, based on suitable modifications of Euler-Bernoulli or Timoshenko beam model coefficients (Banerjee and Williams, 1985, 1986; Friedman and Kosmatka, 1993; Sapountzakis and Panagos, 2008; Shooshtari and Khajavi, 2010),
- enhanced models, that consider an accurate description of stress (Rubin, 1999; Aminbaghai and Binder, 2006) and are often derived from variational principles (Hodges et al., 2008, 2010; Auricchio et al., 2015; Beltempo et al., 2015),
- models based on 2D or 3D Finite Elements (FE), that often appear as the only possible path, especially when an accurate description of unknown fields is required (Kechter and M.Gutkowski, 1984; El-Mezaini et al., 1991; Balkaya, 2001).

It is well known since the half of the past century that the simple models are no-longer effective in predicting the real behavior of non-prismatic beams (Boley, 1963; Hodges et al., 2010). On the other hand, 2D FE models lead to a high computational effort. As a consequence, the enhanced models seem the best compromise.

It is worth noting that non-prismatic beams are often treated as beams of variable cross-section. In fact, both researchers and practitioners neglect the effects of the non-straight center-line for modeling simplicity (Portland Cement Associations, 1958; Timoshenko and Young, 1965; El-Mezaini et al., 1991; Tena-Colunga, 1996; Balkaya and Citipitioglu, 1997; Ozay and Topcu, 2000). To the author's knowledge, the few attempts of a complete modeling of non-prismatic beams are Balduzzi (2013); Auricchio et al. (2015); Beltempo (2013); Beltempo et al. (2015) that use mixed variational principles and the dimension reduction method to derive

planar beam models and Gimena et al. (2008b) that proposes a model for 3D non-prismatic beams and an effective numerical procedure for the resolution of the Ordinary Differential Equations (ODEs) governing the beam model. Unfortunately, the dimension reduction leads to equations with an unclear physical meaning and a complexity which seems scarcely manageable. Conversely, the model proposed by Gimena et al. (2008b) presents some limitations that will be discussed in the following.

The present paper aims at discussing a simple and effective non-prismatic planar beam model. The derivation procedure is based on a rigorous treatment of the 2D elastic problem and exploits the simple Timoshenko kinematics (i.e., planar cross-section remain planar in consequence of a deformation, but can rotate with respect to the beam center-line). The simplicity of resulting ODEs allows to provide the analytical solution for tapered beams and helps the understanding of several aspects that influence the effectiveness of the non-prismatic beam modeling.

The outline of the paper is as follows. Section 2 introduces the 2D elastic problem we are going to tackle, Section 3 illustrates how to derive the non-prismatic beam model equations, Section 4 focuses on tapered beams for which some analytical results are provided and compared with other approaches existing in literature, Section 5 provides few numerical examples that highlight critical aspects and advantages of the proposed approach, and Section 6 discusses the final remarks and delineates future research's developments.

2. 2D problem formulation

The object of our study is the 2D non-prismatic beam that behaves under the hypothesis of small displacements and plane stress state. Moreover, the material that constitutes the beam body is homogeneous, isotropic, and linear-elastic.

We introduce the beam *longitudinal axis* L, defined as follows

$$L := \{x \in [0, l]\} \tag{1}$$

where l is the *beam length*. Moreover, we define the *beam center-line* $c : L \to \mathbb{R}$ and the *cross-section height* $h : L \to \mathbb{R}^+$ where $\mathbb{R}^+$ indicates strictly positive real values. As usual in prismatic beam modeling, we assume that $l \gg h(x) \, \forall x \in L$ noting that this ratio plays a central role in determining the model accuracy. Furthermore, we assume that the beam longitudinal axis and the beam center-line are reasonably next to each other, this recommendation will become more clear in Section 4.3.2. Finally, we assume that $c(x)$ and $h(x)$ are sufficiently smooth functions which properties will be detailed in the following.

The *cross-section lower and upper limits*, $h_l, h_u : L \to \mathbb{R}$ are defined as follows

$$h_l(x) := c(x) - \frac{1}{2}h(x); \quad h_u(x) := c(x) + \frac{1}{2}h(x) \tag{2}$$

Therefore, the *cross-section* $A(x)$ is defined as follows

$$A(x) := \{y | \text{ given } x \in L \Rightarrow y \in [h_l(x), h_u(x)]\} \tag{3}$$

It is worth noting that Definition (3) introduces a small notation abuse: $A(x)$ is a set and not a function. Nevertheless, it highlights the dependence of set definition on the axis coordinate. Furthermore, Definition (3) leads to cross-sections $A(x)$ that are orthogonal to the longitudinal axis and not to the beam center-line, according to the approach proposed by Gimena et al. (2008a).

Using all the so far introduced notations, the 2D *problem domain* Ω results defined as follows

$$\Omega := \{(x, y) | \forall x \in L \rightarrow y \in A(x)\} \tag{4}$$

Figure 1 represents the 2D domain Ω, the adopted Cartesian coordinate system Oxy, the lower and upper limits $y = h_l(x)$ and $y = h_u(x)$, the center-line $y = c(x)$, the longitudinal axis L, the *initial* and the *final cross-sections* $A(0)$ and $A(l)$.

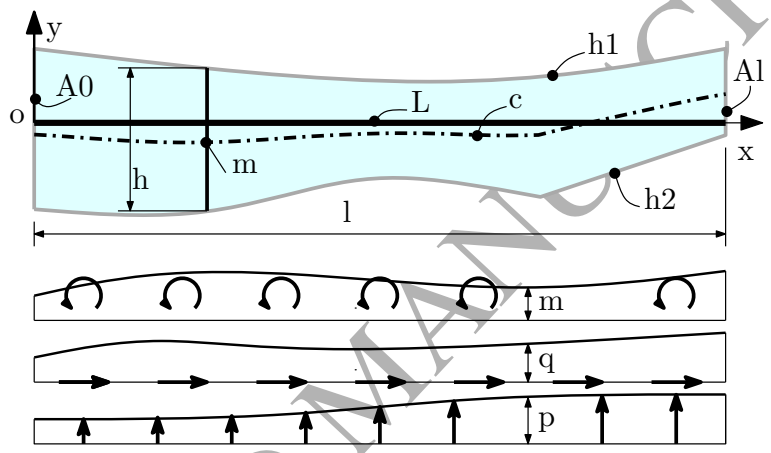

Figure 1: Beam geometry, problem domains, coordinate system, dimensions, resulting loads, and adopted notations.

We denote the *domain boundary* as $\partial\Omega$, such that $\partial\Omega := A(0) \cup A(l) \cup h_l(x) \cup h_u(x)$. Moreover, we introduce the partition $\{\partial\Omega_s; \partial\Omega_t\}$, where $\partial\Omega_s$ and $\partial\Omega_t$ are the displacement constrained and the loaded boundaries, respectively.

As usual in beam modeling, we assume that the lower and upper limits belong to the loaded boundary (i.e., $h_l(x)$ and $h_u(x) \in \partial\Omega_t$) whereas al least one of the initial and final cross-sections $A(0)$ and $A(l)$ belong to the displacement constrained boundary $\partial\Omega_s$ that can not be an empty set in order to ensure solution uniqueness. The boundary load distribution $\boldsymbol{t} : \partial\Omega_t \rightarrow \mathbb{R}^2$ is assumed to vanish on lower and upper limits (i.e., $\boldsymbol{t}|_{h_{l,u}} = \boldsymbol{0}$). It is worth noting that this hypothesis is not strictly necessary to the beam model derivation and therefore it can be removed with suitable modifications of the model equations. Finally, a distributed load $\boldsymbol{f} : \Omega \rightarrow \mathbb{R}^2$ is applied to the beam body and a suitable boundary displacement function $\overline{\boldsymbol{s}} : \partial\Omega_s \rightarrow \mathbb{R}^2$ is assigned in order to opportunely reproduce the constraint usually adopted in structural mechanics.

We highlight that the proposed geometry formulation is as general as possible and recovers easily both the cases of curved beam and beam of variable cross-section, assuming respectively that $h(x)$ or $c(x)$

are constant. Furthermore, with respect to the classical definition of curved beams (Capurso, 1971), the proposed approach does not require conditions on center-line's second derivative. Conversely, the proposed approach can tackle only center-lines and thickness with bounded first derivatives, for reasons that will be more clear in the following. This could be a limit since –as an example– the proposed method does not have the capability to describe a semi-circular beam. Nevertheless, the so far highlighted limitation can be easily bypassed through the use of approximations or simple tricks.

We introduce the *stress* field $\boldsymbol{\sigma} : \Omega \to \mathbb{R}^{2\times 2}_s$, the *strain* field $\boldsymbol{\varepsilon} : \Omega \to \mathbb{R}^{2\times 2}_s$, and the *displacement vector* field $\boldsymbol{s} : \Omega \to \mathbb{R}^2$, where $\mathbb{R}^{2\times 2}_s$ denotes the space of symmetric, second order tensors. Thereby, the 2D elastic problem corresponds to the following boundary value problem

$$\boldsymbol{\varepsilon} = \nabla^s \boldsymbol{s} \qquad \text{in} \quad \Omega \tag{5a}$$

$$\boldsymbol{\sigma} = \boldsymbol{D} : \boldsymbol{\varepsilon} \qquad \text{in} \quad \Omega \tag{5b}$$

$$\nabla \cdot \boldsymbol{\sigma} + \boldsymbol{f} = \boldsymbol{0} \qquad \text{in} \quad \Omega \tag{5c}$$

$$\boldsymbol{\sigma} \cdot \boldsymbol{n} = \boldsymbol{t} \qquad \text{on} \quad \partial\Omega_t \tag{5d}$$

$$\boldsymbol{s} = \overline{\boldsymbol{s}} \qquad \text{on} \quad \partial\Omega_s \tag{5e}$$

where $\nabla^s(\,\cdot\,)$ is the operator that provides the symmetric part of the gradient, $\nabla\cdot(\,\cdot\,)$ represents the divergence operator, $(\,\cdot\,):(\,\cdot\,)$ represents the double dot product, and $\boldsymbol{D}$ is the fourth order tensor that defines the mechanical properties of the material. Equation (5a) is the 2D *compatibility* relation, Equation (5b) is the 2D *material constitutive relation*, and Equation (5c) represents the 2D *equilibrium* relation. Equations (5d) and (5e) are respectively the *boundary equilibrium* and the *boundary compatibility* conditions, where $\boldsymbol{n}$ is the outward unit vector, defined on the boundary.

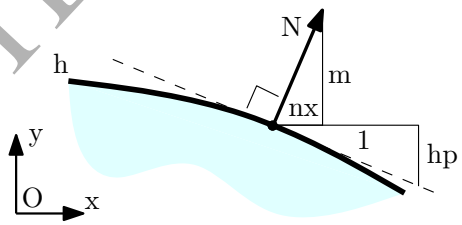

Figure 2: Outward unit vector evaluated on the upper limit function $h'_u(x)$.

As illustrated in Figure 2, the outward unit vectors on the lower and upper limits result as follows

$$\boldsymbol{n}|_{h_l}(x) = \frac{1}{\sqrt{1+(h'_l(x))^2}} \begin{Bmatrix} h'_l(x) \\ -1 \end{Bmatrix}; \quad \boldsymbol{n}|_{h_u}(x) = \frac{1}{\sqrt{1+(h'_u(x))^2}} \begin{Bmatrix} -h'_u(x) \\ 1 \end{Bmatrix} \tag{6}$$

where $(\,\cdot\,)'$ denotes the derivative with respect to the independent variable x. The boundary equilibrium

(5d) on lower and upper limits (i.e., $(\boldsymbol{\sigma}\cdot\boldsymbol{n})|_{h_l\cup h_u}=\mathbf{0}$) could be expressed as follows

$$\begin{bmatrix} \sigma_x & \tau \\ \tau & \sigma_y \end{bmatrix} \begin{Bmatrix} n_x \\ n_y \end{Bmatrix} = \begin{Bmatrix} 0 \\ 0 \end{Bmatrix} \quad \Rightarrow \quad \begin{cases} \sigma_x n_x + \tau n_y = 0 \\ \tau n_x + \sigma_y n_y = 0 \end{cases} \tag{7}$$

where we omit the indication of the restriction $(\cdot)|_{h_l\cup h_u}$ for notation simplicity. Manipulating Equation (7), we express τ and σ_y as function of σ_x; using the outward unit vector $\boldsymbol{n}$ definition (6), we obtain the following expressions for boundary equilibrium

$$\tau = -\frac{n_x}{n_y}\sigma_x = h'\sigma_x \tag{8a}$$

$$\sigma_y = \frac{n_x^2}{n_y^2}\sigma_x = (h')^2\,\sigma_x \tag{8b}$$

where h indicates either $h_l(x)$ or $h_u(x)$, accordingly to the point where we are evaluating the function. Equation (8) is defined only for non-vanishing n_y, therefore we need to require that first derivatives of lower and upper limits –and consequently of center-line and cross-section height– are bounded.

As already highlighted in (Auricchio et al., 2015), σ_x could be seen as the independent variable that completely defines the stress state on the lower and upper surfaces. Moreover, as stated by Boley (1963) and Hodges et al. (2008, 2010) the lower and upper limit slopes h_l' and h_u' play a central role in boundary equilibrium, determining the stress distribution within the cross-section $A(x)$.

3. Simplified 1D model

This section aims at deriving the ODEs representing the beam model. In fact, the solution of the 2D problem introduced in Section 2 is in general not available. As a consequence, in order to obtain an approximated solution, practitioners consider simplified models properly called *beam models*. The non-prismatic beam model derivation consists of 4 main steps

1. derivation of compatibility equations,
2. derivation of equilibrium equations,
3. stress representation, and
4. derivation of simplified constitutive relations

that correspond to the subdivision of the present section.

Figure 1 represents the domain of the beam model we are going to develop. It is worth noting that Equation (5) considers a 2D region as problem domain, the classical curved beam models considers the center-line $c(x)$, and the beam model we are going to develop considers the beam axis L. Furthermore, we remark that all the generalized variables we are going to use are referred to the global Cartesian coordinate system Oxy.

In Figure 1, $q(x)$, $m(x)$, and $p(x)$ are the *horizontal*, *bending*, and *vertical resulting loads* defined as

$$q(x) = \int_{A(x)} f_x(x,y)\, dy; \quad m(x) = -\int_{A(x)} y f_x(x,y)\, dy; \quad p(x) = \int_{A(x)} f_y(x,y)\, dy \tag{9}$$

where $f_x(x,y)$ and $f_y(x,y)$ are the horizontal and vertical components of the load vector $\boldsymbol{f}$.

Finally, for convenience during the model derivation, we introduce the linear function $\tilde{b}(y)$ defined as

$$\tilde{b}(y) = \frac{2(c(x) - y)}{h(x)} \tag{10}$$

We note that $\tilde{b}(y)$ represents an odd function with respect to the cross-section $A(x)$, it vanishes at $y = c(x)$, and it is equal to ± 1 at $y = h_{u/l}(x)$.

3.1. Compatibility equations

In order to develop the non-prismatic beam model, we assume that the kinematics usually adopted for prismatic Timoshenko beam models is still valid. Therefore, we represent 2D displacement field $\boldsymbol{s}(x,y)$ in terms of three 1D functions indicated as *generalized displacements*: the *horizontal displacement* $u(x)$, the *rotation* $\varphi(x)$, and the *vertical displacement* $v(x)$. Specifically, we assume that the beam body displacements are approximated as follows:

$$\boldsymbol{s}(x,y) \approx \left\{ \begin{array}{c} u(x) - \dfrac{h(x)}{2}\tilde{b}(y)\,\varphi(x) \\ v(x) \end{array} \right\} \tag{11}$$

We introduce the *generalized deformations* i.e., the *horizontal deformation* $\varepsilon_0(x)$, the *curvature* $\chi(x)$, and the *shear deformation* $\gamma(x)$ respectively defined as follows

$$\varepsilon_0(x) = \frac{1}{h(x)} \int_{A(x)} \varepsilon_x dy; \quad \chi(x) = \frac{12}{h^3(x)} \int_{A(x)} \varepsilon_x (c(x) - y)\, dy; \quad \gamma(x) = \frac{1}{h(x)} \int_{A(x)} \varepsilon_{xy} dy \tag{12}$$

where ε_x and ε_{xy} are the components of the strain tensor $\boldsymbol{\varepsilon}$.

Therefore, the beam compatibility is expressed through the following equations

$$\varepsilon_0(x) = u'(x) - c'(x)\,\varphi(x) \tag{13a}$$

$$\chi(x) = -\varphi'(x) \tag{13b}$$

$$\gamma(x) = v'(x) + \varphi(x) \tag{13c}$$

We note that, with respect to the prismatic beam compatibility, a new term $c'(x)\,\varphi(x)$ appears in Equation (13a). Its physical meaning is illustrated in Figure 3 that shows that, if the center-line is non-horizontal, a rotation induces non-negligible horizontal displacement. On the other hand, considering a straight center-line parallel to the beam axis, this term vanishes recovering the more familiar compatibility equations usually adopted for prismatic beams.

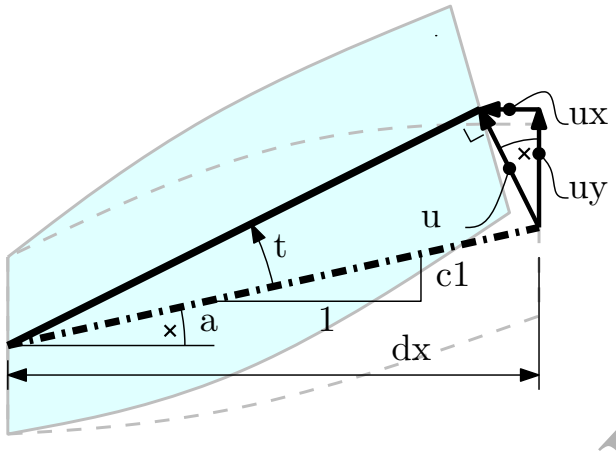

Figure 3: Schematic representation of displacements induced by rotation.

3.2. Equilibrium equations

We introduce the *generalized stresses* i.e., the *resulting horizontal stress* $H(x)$, the *resulting bending moment* $M(x)$, and the *resulting vertical stress* $V(x)$ respectively defined as follows

$$H(x) = \int_{A(x)} \sigma_x dy \tag{14a}$$

$$M(x) = \int_{A(x)} \sigma_x (c(x) - y)\, dy \tag{14b}$$

$$V(x) = \int_{A(x)} \tau dy \tag{14c}$$

We use the virtual work principle in order to obtain the beam equilibrium equations. The internal work $\mathcal{L}_{int}$ can be calculated multiplying the virtual generalized deformations $\delta\varepsilon_0(x)$, $\delta\chi(x)$, and $\delta\gamma(x)$ (that satisfy Equation (13)) for the corresponding equilibrated generalized stresses $H(x)$, $M(x)$, and $V(x)$. Analogously, the external work $\mathcal{L}_{ext}$ can be calculated multiplying the virtual generalized displacements $\delta u(x)$, $\delta\varphi(x)$, and $\delta v(x)$ for the corresponding resulting loads. Equalizing internal and external works we obtain

$$\begin{aligned} \mathcal{L}_{int} &= \int_L \left[\delta\varepsilon_0(x) \cdot H(x) + \delta\chi(x) \cdot M(x) + \delta\gamma(x) \cdot V(x)\right] dx = \\ \mathcal{L}_{ext} &= \int_L \left[\delta u(x) \cdot q(x) - \delta\varphi(x) \cdot m(x) + \delta v(x) \cdot p(x)\right] dx \end{aligned} \tag{15}$$

Substituting compatibility equations (13) in Equation (15) we obtain:

$$\begin{aligned} &\int_L \left[\left[\delta u'(x) - c'(x)\,\delta\varphi(x)\right] \cdot H(x) - \delta\varphi'(x) \cdot M(x) + \left[\delta v'(x) + \delta\varphi(x)\right] \cdot V(x)\right] dx = \\ &\int_L \left[\delta u(x) \cdot q(x) - \delta\varphi(x) \cdot m(x) + \delta v(x) \cdot p(x)\right] dx \end{aligned} \tag{16}$$

Integrating by parts the terms that apply derivatives to virtual generalized displacements and later collecting

generalized displacements, we obtain

$$-\int_L \delta u\,(x)\cdot H'\,(x)\,dx+\int_L \delta\varphi\,(x)\cdot\left[M'-c'\,(x)\,H\,(x)+V\,(x)\right]dx-\int_L \delta v\,(x)\cdot V'\,(x)\,dx=$$
$$\int_L \left(\delta u\,(x)\cdot q\,(x)-\delta\varphi\,(x)\cdot m\,(x)+\delta v\,(x)\cdot p\,(x)\right)dx \tag{17}$$

In order to satisfy Equation (17) for all possible virtual generalized displacements, generalized stresses must satisfy the following equations

$$H'\,(x)=-q\,(x) \tag{18a}$$
$$M'\,(x)-H\,(x)\cdot c'\,(x)+V\,(x)=-m\,(x) \tag{18b}$$
$$V'\,(x)=-p\,(x) \tag{18c}$$

that therefore are the equilibrium relations.

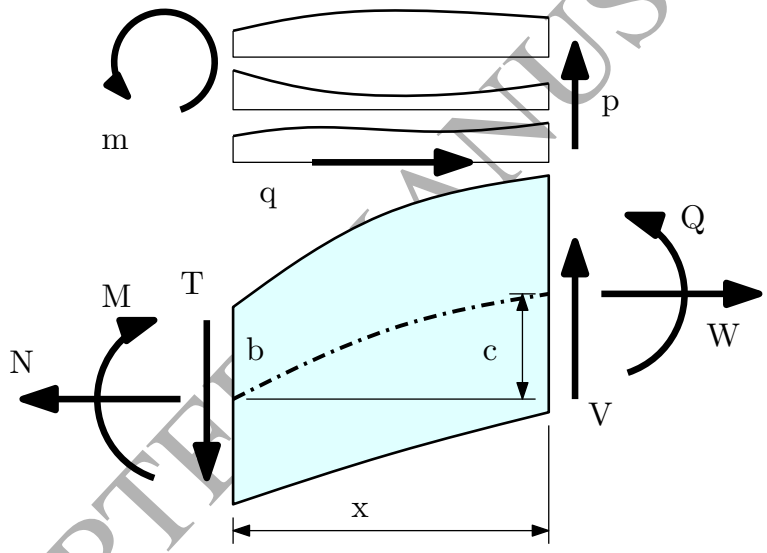

Figure 4: Resulting loads and generalized stresses acting on a portion of non-prismatic beam of length dx.

It is worth noting that equilibrium equations (18) can be obtained considering the equilibrium of a portion of non-prismatic beam of length dx (see Figure 4). Furthermore, Equation (18b) is a generalization of prismatic beam rotation equilibrium. Specifically, the term $H\,(x)\cdot c'\,(x)$ takes into account the moment induced by horizontal resulting forces that are applied at different y coordinate in each cross-sections. As expected, the coefficient $c'\,(x)$ vanishes for prismatic beams, leading to the well known prismatic beam equilibrium equation.

3.3. Recovery of cross-section stress distributions

The Timoshenko beam recovers the stress distributions within the cross-section through the following assumptions:

- the horizontal stress σ_x has a linear distribution,
- the vertical stress σ_y has a vanishing value,
- the shear stress τ has a parabolic distribution, according to Jourawski theory (Timoshenko, 1955, Chapter IV).

Beltempo et al. (2015) apply the so far introduced hypotheses to several non-prismatic beams demonstrating that (i) the assumption on horizontal stress seems reasonable in all the considered cases (ii) the Jourawski theory is completely ineffective in predicting the real shear stress distribution since it leads to violate the boundary equilibrium (8a) on $h_l(x)$ and $h_u(x)$.

Therefore, we modify the recovery of cross-section shear-stress distribution as illustrated in Figure 5. Specifically, given the generalized stresses $H(x)$ and $M(x)$ it is possible to reconstruct the horizontal stress

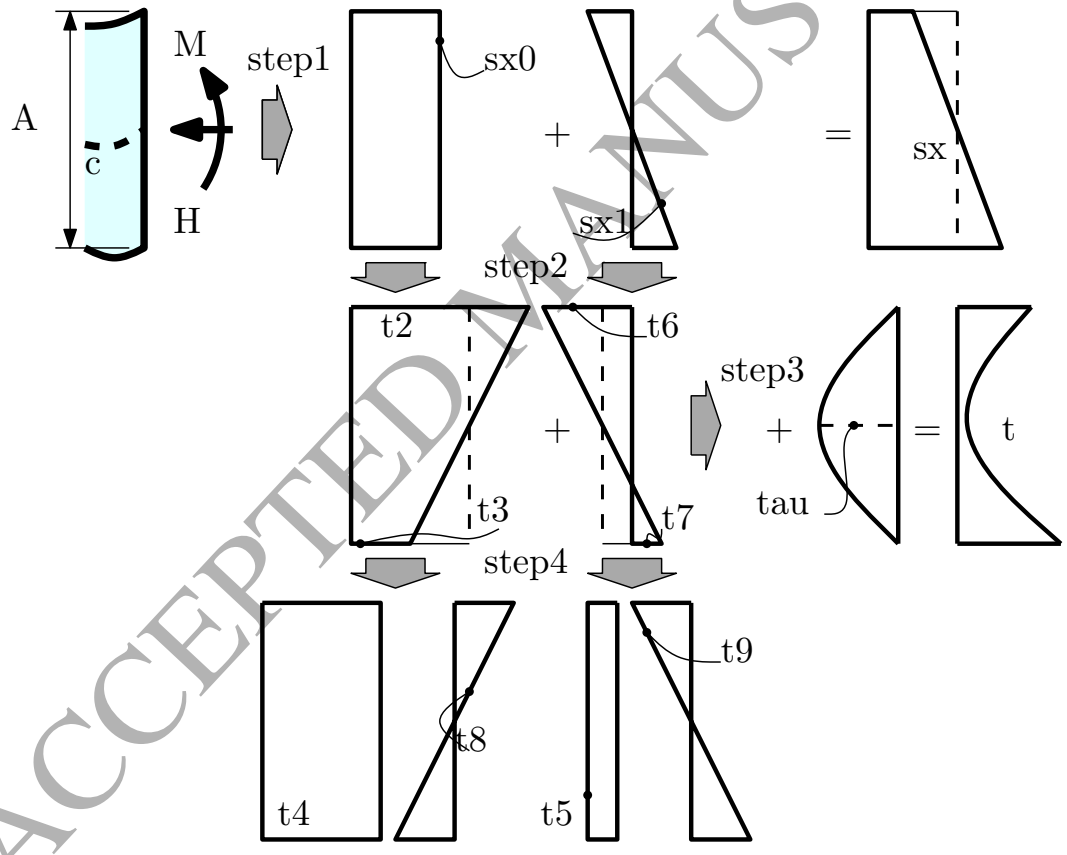

Figure 5: Procedure for the reconstruction of cross-section stress distributions. Step 1: reconstruction of horizontal stress distribution. Step 2: evaluation of shear stresses at the cross-section boundaries and interpolation. Step 3: superimposition of a bouble function in order to satisfy Equation (14c). Step 4: decomposition of shear components in odd and even contributions.

distribution within the cross-section and, in particular, to evaluate the horizontal stress magnitude on lower and upper limits $h_l(x)$ and $h_u(x)$ (Step 1). Boundary equilibrium (8a) allows to evaluate the shear stress

at lower and upper limits of the cross-section $-\tau|_{h_l}$ and $\tau|_{h_u}$ respectively– that thereafter we interpolate through linear functions (Step 2). In order to satisfy Equations (14c) we add a bubble function to the linear shear stress distribution obtaining a parabolic shear stress distribution (Step 3). Finally, we decompose the linear shear stress distributions in odd and even contributions (Step 4).

Recalling the h_l and h_u definitions (2) and performing simple calculations, the stress distributions result as follows

$$\sigma_x(x,y) = \sigma_{x0}(x) + \tilde{b}(y) \cdot \sigma_{x1}(x) \tag{19a}$$

$$\begin{aligned}\tau(x,y) =& c'(x)\,\sigma_{x0}(x) - \frac{h'(x)}{2}\sigma_{x1}(x) + \\ &\left(-\frac{h'(x)}{2}\sigma_{x0}(x) + c'(x)\,\sigma_{x1}(x)\right)\tilde{b}(y) + \frac{3}{2}\widetilde{\tau}(x)\left(1-\tilde{b}^2(y)\right)\end{aligned} \tag{19b}$$

where the variables $\sigma_{x0}(x)$, $\sigma_{x1}(x)$, and $\widetilde{\tau}(x)$ result defined as follows

$$\sigma_{x0}(x) = \frac{H(x)}{h(x)}; \quad \sigma_{x1}(x) = M(x)\frac{6}{h^2(x)}; \quad \widetilde{\tau}(x) = \left(-\frac{V(x)}{h(x)} - c'(x)\,\sigma_{x0}(x) + \frac{h'(x)}{2}\sigma_{x1}(x)\right) \tag{20}$$

Finally, few algebraic steps allow us to express the shear stress distribution as illustrated in the following

$$\begin{aligned}\tau(x,y) =& \left(c'(x)\,\sigma_{x0}(x) - \frac{h'(x)}{2}\sigma_{x1}(x)\right)\left(-\frac{1}{2} + \frac{3}{2}\tilde{b}^2(y)\right) \\ &- \left(\frac{h'(x)}{2}\sigma_{x0}(x) - c'(x)\,\sigma_{x1}(x)\right)\tilde{b}(y) + \frac{3}{2}\tau_0(x)\left(1-\tilde{b}^2(y)\right)\end{aligned} \tag{21}$$

where the variable $\tau_0(x)$ results defined as follows

$$\tau_0(x) = -\frac{V(x)}{h(x)} \tag{22}$$

It is worth noting that the previously introduced quantities have a clear physical meaning:

- $\sigma_{x0}(x)$ is the mean value of the horizontal stress within the cross-section,
- $\sigma_{x1}(x)$ is the maximum horizontal stress value induced by bending moment that occurs at the cross-section lower limit, and
- $\tau_0(x)$ is the shear stress mean value.

In Equation (21), the shear distribution τ depends not only on $V(x)$, but also on $H(x)$ and $M(x)$ that determine not only the magnitude but also the shape of the shear distribution. Finally, Equation (21) leads to conclude that the maximum shear stress does not occur in correspondence of the beam center-line, as noted by Paglietti and Carta (2007, 2009).

The assumption of vanishing vertical stresses $\sigma_y(x,y) = 0$ agrees with the assumptions of prismatic beam stress recovery, significantly simplifying the beam model equations, but leads to violate Equation (8b). Fortunately, this choice will not deeply worsen the model capability, as the numerical examples of

Section 5 will illustrate. On the other hand, readers may refer to (Auricchio et al., 2015; Beltempo et al., 2015) for more refined models that do not neglect the contribution of vertical stresses.

The recovery relation (21) is well known since the first half of the twentieth century. In particular, referring to the analytical solution of the 2D equilibrium equation (5c) for an infinite long wedge, Atkin (1938); Cicala (1939); Timoshenko and Goodier (1951) express the stress distribution as the combination of some trigonometric functions. More in detail, Timoshenko and Goodier (1951) state that a parabolic shear distribution is an approximation reasonably accurate in the case of small boundary slope. Later on, Krahula (1975) extends the so far mentioned results to tapered beams, recovering equations substantially identical to (19a) and (21). Furthermore, more recently, Bruhns (2003, Example 3.9) notes that (i) the shear distribution in a tapered beam has no longer a distribution similar to the prismatic beams, (ii) the shear distribution depends not only on resulting shear, but also in bending moment and resulting horizontal stress, and (iii) the maximum shear could occur everywhere in the cross-section.

However, it is worth noting that all the so far mentioned references consider the stress representation (19a) and (21) valid only for tapered beams whereas we are extending the representation's validity to more general cases. The numerical examples reported in (Auricchio et al., 2015; Beltempo et al., 2015) partially confirm that the recovery relations (19a) and (21) remain valid also in more general situations. Obviously, the effectiveness of stress description as well as of the beam model will decrease increasing the boundary slope and decreasing the beam slenderness, as it happens for tapered beams.

3.4. Simplified constitutive relations

To complete the Timoshenko-like beam model we need to introduce some simplified constitutive relations that define the generalized deformations as a function of generalized stresses.

The constitutive relation of the Timoshenko prismatic beam model needs a correction factor k that is introduced in order to equalize the work of generalized shear stresses and deformations that considers only their mean values and the work of real shear stresses and strains that takes into account the real stress and strain distributions within the cross-section. In particular, for the simple case of a rectangular cross-section, the shear correction factor could be evaluated through the following formula

$$k = \frac{\int_A \frac{1}{G}\tau^2 dy}{h\left(x\right)\frac{1}{G}\frac{V^2(x)}{h^2(x)}} = \frac{1}{h\left(x\right)}\int_A \frac{9}{4}\left(1-\tilde{b}^2\left(y\right)\right)^2 dy = \frac{5}{6} \tag{23}$$

It is worth noting that Equation (23) is effective because only the magnitude varies while the shear distribution has the same shape in all the cross-sections. Unfortunately, this does not hold for the non-prismatic beam. This simple consideration, together with the non trivial dependence $\tau\left(x,y\right)$ on $H\left(x\right)$ and $M\left(x\right)$ –see Equation (21)– lead to conclude that the prismatic beam constitutive relations are not satisfactory for the non-prismatic beams and a more refined approach must be adopted.

In particular, we consider the stress potential, defined as follows

$$\Psi^* = \frac{1}{2}\left(\frac{\sigma_x^2(x,y)}{E} + \frac{\tau^2(x,y)}{G}\right) \tag{24}$$

where E is the Young's modulus and G is the shear modulus. Substituting the stress recovery relations (19a) and (21) in Equation (24), the generalized deformations result as the derivatives of the stress potential with respect to the corresponding generalized stress. Therefore we have

$$\varepsilon_0(x) = \int_{A(x)} \frac{\partial \Psi^*}{\partial H(x)} dy = \varepsilon_H H(x) + \varepsilon_M M(x) + \varepsilon_V V(x) \tag{25a}$$

$$\chi(x) = \int_{A(x)} \frac{\partial \Psi^*}{\partial M(x)} dy = \chi_H H(x) + \chi_M M(x) + \chi_V V(x) \tag{25b}$$

$$\gamma(x) = \int_{A(x)} \frac{\partial \Psi^*}{\partial V(x)} dy = \gamma_H H(x) + \gamma_M M(x) + \gamma_V V(x) \tag{25c}$$

where

$$\varepsilon_H = \left(\frac{c'^2(x)}{5Gh(x)} + \frac{h'^2(x)}{12Gh(x)} + \frac{1}{Eh(x)}\right); \qquad \varepsilon_M = \chi_H = -\frac{8c'(x)h'(x)}{5Gh^2(x)}; \qquad \varepsilon_V = \gamma_H = \frac{c'(x)}{5Gh(x)}$$

$$\chi_M = \left(\frac{9h'^2(x)}{5Gh^3(x)} + \frac{12c'^2(x)}{Gh^3(x)} + \frac{12}{Eh^3(x)}\right); \qquad \chi_V = \gamma_M = -\frac{3h'(x)}{5Gh^2(x)}; \qquad \gamma_V = \frac{6}{5Gh(x)}$$

It is worth noting the following statements.

- Unlike the prismatic beam models, the generalized deformations depend on all generalized stresses.
- It is possible to recognize in ε_H, χ_M, and γ_V the terms of prismatic beam constitutive laws

$$\varepsilon_0(x) = \frac{H(x)}{Eh(x)}; \quad \chi(x) = \frac{12M(x)}{Eh^3(x)}; \quad \gamma(x) = -\frac{V(x)}{kGh(x)} \tag{26}$$

- The shear correction factor, as well as the other coefficients, results naturally from the derivation procedure, bypassing the problem of their evaluation.

To the author's knowledge, Vu-Quoc and Léger (1992) are the former researchers mentioning the non-trivial dependence of all generalized deformations on all generalized stresses. Considering the shear bending of a tapered beam, the authors derive the beam's flexibility matrix using the principle of complementary virtual work. Later on, deriving a model for a tapered beam, Rubin (1999) and Aminbaghai and Binder (2006) consider the fact that the bending moment produces also shear deformation and the shear force produces a curvature. Unfortunately, they do not consider the effect of a non-horizontal center-line and Rubin (1999) use different coefficients with respect to the ones reported in Equations (25), resulting energetically inconsistent. Conversely, for the model derivation, Hodges et al. (2008); Auricchio et al. (2015); Beltempo et al. (2015) use variational principles that have the advantage to naturally derive the constitutive relations, but could lead to more complicated equations, as already highlighted in Section 1.

3.5. Remarks on beam model's ODEs

In the following we resume the beam model's ODEs according to the notation adopted by Gimena et al. (2008a).

$$\begin{Bmatrix} H'(x) \\ V'(x) \\ M'(x) \\ \varphi'(x) \\ v'(x) \\ u'(x) \end{Bmatrix} = \left[\begin{array}{ccc|ccc} 0 & 0 & 0 & & & \\ 0 & 0 & 0 & & \mathbf{0} & \\ -c'(x) & 1 & 0 & & & \\ \hline \chi_H & \chi_V & \chi_M & 0 & 0 & 0 \\ \gamma_H & \gamma_V & \gamma_M & 1 & 0 & 0 \\ \varepsilon_H & \varepsilon_V & \varepsilon_M & -c'(x) & 0 & 0 \end{array}\right] \begin{Bmatrix} H(x) \\ V(x) \\ M(x) \\ \varphi(x) \\ v(x) \\ u(x) \end{Bmatrix} - \begin{Bmatrix} q(x) \\ p(x) \\ m(x) \\ 0 \\ 0 \\ 0 \end{Bmatrix} \tag{27}$$

With respect to Equation (27), it is worth noting what follows.

- The equations are naturally expressed as an explicit system of first order ODEs.
- Similar to Gimena et al. (2008a), the matrix that collects equations' coefficients has a lower triangular form with vanishing diagonal terms. As a consequence, the analytical solution can easily be obtained through an iterative process of integration done row by row, starting from $H(x)$ and arriving at $u(x)$.
- Reducing the beam model proposed by Gimena et al. (2008a) to a 2D case, it is easy to recognize the same structure in equilibrium and kinematics relations. Specifically Gimena et al. (2008a) use trigonometric coefficients whereas we use the corresponding linearized ones (i.e., we assume that $\sin(\theta) \approxeq \tan(\theta) \approxeq \theta$).
- The sub-matrix that collects the constitutive relation coefficients is symmetric with respect to the anti-diagonal.
- Finally, the sub-matrix that collects the constitutive relation coefficients is completely full whereas Gimena et al. (2008a) neglect coupling between curvature, horizontal, and vertical resulting stresses (i.e., $\chi_H = \chi_V = \varepsilon_M = \gamma_M = 0$). Examples reported in Section 5 will illustrate that all the terms of the simplified constitutive relations plays a crucial role and are in general not negligible.

Now we move our attention back to the equilibrium (18) and the compatibility (13) equations. It is worth noting that the use of a global Cartesian coordinate system presents the following main advantages.

- Both the beam equilibrium and compatibility are not influenced by the cross-section size, which on the contrary plays a central role in constitutive relations.
- Horizontal and vertical equilibrium are expressed through independent equations, whereas in classical formulation (Bruhns, 2003, Chapter 5) tangential and normal equilibrium equations are coupled.

Furthermore, we note that few researchers follow the path of using a global Cartesian coordinate system with cross-sections orthogonal to $x-$ axis. Fung and Kaplan (1952) investigate the buckling of beams with small curvatures and Borri et al. (1992); Popescu et al. (2000); Rajagopal and Hodges (2014) propose beam models considering oblique cross-sections. On the other hand, Vogel (1993) develops a second order Euler-Bernoulli beam model for curved beams in large displacement regime and Gimena et al. (2008a,b) develop 3D non-prismatic beam models expressing the resulting forces in a global coordinate system.

Finally, if we neglect shear deformation in the proposed model and the second order terms in (Vogel, 1993) –i.e., if we lead both models to use the same assumptions– we obtain the same equations, showing once more that the proposed model has the capability to recover simpler models available in literature.

4. Tapered beam analytical solution

This section discusses the analytical solution of the ODEs governing the problem (27) for the simple case of a tapered beam. Specifically, we consider a beam with an inclined center-line, as illustrated in Figure 6.

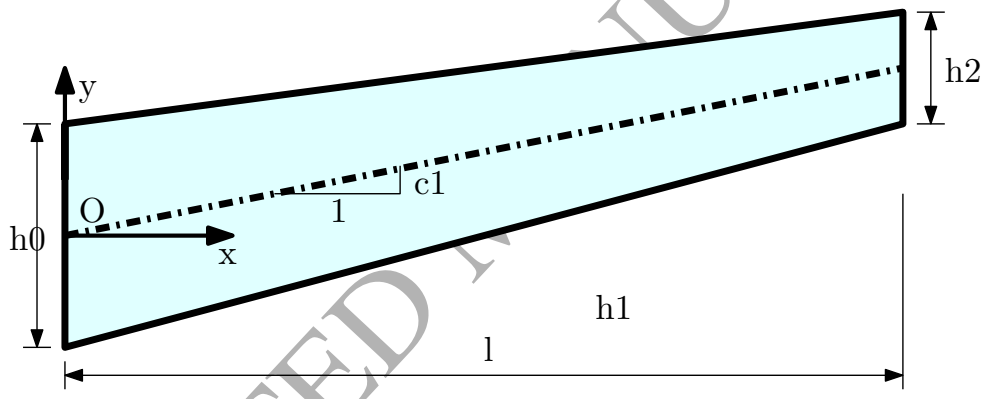

Figure 6: Tapered beam considered for the evaluation of the analytical solution: geometry and parameter's definitions.

The center-line and the thickness have the following analytical expressions

$$c\left(x\right) = c_1 x; \quad h\left(x\right) = h_1 x + h_0 \tag{28}$$

4.1. Homogeneous solution

Considering the geometry so far introduced, the homogeneous solution of the beam model ODEs (27) is

$$
\begin{aligned}
H(x) =& C_6 \\
M(x) =& (c_1 C_6 - C_5)\, x + C_4 \\
V(x) =& C_5 \\
\varphi(x) =& -\frac{3\left(20Ec_1^2 + 3Eh_1^2 + 20G\right)}{10EGh_1^2 h^2(x)} \left(h_0 (c_1 C_6 - C_5) - h_1 C_4\right) \\
&+ \frac{c_1\left(60Ec_1^2 + Eh_1^2 + 60G\right)}{5EGh_1^2 h(x)} C_6 - \frac{6\left(10Ec_1^2 + Eh_1^2 + 10G\right)}{5EGh_1^2 h(x)} C_5 + C_3 \\
u(x) =& \frac{\log(h(x))}{60EGh_1^3}\left(72c_1\left(10Ec_1^2 - Eh_1^2 + 10G\right)(c_1 C_6 - C_5) + 5h_1^2 (Eh_1 + 12G) C_6 + 12c_1 Eh_1^2 C_5\right) \\
&- \frac{c_1\left(60Ec_1^2 - 7Eh_1^2 + 60G\right)}{10EGh_1^3 h(x)} \left(h_0 (C_5 - c_1 C_6) + h_1 C_4\right) \\
&+ c_1 x C_3 + C_2 \\
v(x) =& -\frac{\log(h(x))}{5EGh_1^3}\left(c_1\left(60Ec_1^2 - Eh_1^2 + 60G\right) C_6 - 3\left(20Ec_1^2 + 3Eh_1^2 + 20G\right) C_5\right) \\
&- \frac{3\left(20Ec_1^2 + Eh_1^2 + 20G\right)}{10EGh_1^3 h(x)} \left(c_1 h_0 C_6 - h_0 C_5 - h_1 C_4\right) - x C_3 + C_1
\end{aligned}
\tag{29}
$$

where the parameters C_1, C_2, C_3, C_4, C_5, and C_6 depend on boundary conditions.

The analytical solution of non-prismatic beam (29) uses rational and logarithmic terms whereas the analytical solution of prismatic beam uses polynomial terms. As a consequence, the polynomials usually adopted in structural analysis in order to reconstruct the prismatic beam displacement given the nodal displacements or as shape functions for FE software, are no longer effective for non-prismatic beams. Furthermore, the non-prismatic beam stiffness matrix has a completely different structure that is influenced by the non-trivial distribution of displacements along the beam longitudinal axis and the strong coupling of all equations. The homogeneous solution (29) can be used to overcome these problems, nonetheless these aspects lie outside this paper's aims and will be object of a further scientific paper.

4.2. Particular solution

Considering a constant vertical load $p(x) = p$ we obtain the following particular solution for the beam model ODEs (27).

$$
\begin{aligned}
H(x) =& 0 \\
M(x) =& \frac{1}{2} p x^2 \\
V(x) =& -px \\
\varphi(x) =& -\frac{3p}{20EGh_1^3}\left(2\left(20Ec_1^2+Eh_1^2+20G\right)\log\left(h(x)\right)-\frac{h_0^2\left(20Ec_1^2+3Eh_1^2+20G\right)}{h^2(x)}\right. \\
&\left.+8\frac{h_0\left(10Ec_1^2+Eh_1^2+10G\right)}{h(x)}\right) \\
u(x) =& -\frac{3c_1 p}{10EGh_1^4}\left(\left(20Ec_1^2+Eh_1^2+20G\right)h(x)\left(\log\left(h(x)\right)-1\right)+\frac{4}{3}\left(60Ec_1^2-Eh_1^2+60G\right)h_0\log\left(h(x)\right)\right. \\
&\left.+\left(20Ec_1^2+Eh_1^2+20G\right)h(x)+\frac{h_0^2\left(60Ec_1^2-7Eh_1^2+60G\right)}{6h(x)}+2xEh_1^3\right) \\
v(x) =& \frac{3p}{EGh_1^4}\left(\left(20Ec_1^2+Eh_1^2+20G\right)h(x)\left(\log\left(h(x)\right)-1\right)+4h_0\left(20Ec_1^2+3Eh_1^2+20G\right)\log\left(h(x)\right)\right. \\
&\left.+\frac{1}{2h(x)}\left(20Ec_1^2+Eh_1^2+20G\right)h_0^2-\frac{3xEh_1^3}{10}\right)
\end{aligned}
\tag{30}
$$

4.3. Asymptotic analysis

In this section, we perform some tests in order to evaluate robustness and correctness of the beam model. Specifically we are going to investigate two main aspects:

1. the behavior of the beam solution when the geometry tends to become prismatic,
2. the capability of the beam model to recover the solution of a tapered beam that has the straight axis rotated with respect to the principal Cartesian coordinate system.

We consider a tapered cantilever, clamped in the initial cross-section and loaded with a vertical concentrated force in the final cross-section i.e., $u(0) = \varphi(0) = v(0) = H(l) = M(l) = 0$, and $V(l) = 1\,\mathrm{N}$. Furthermore, we assume the following values:

$$
l = 10\,\mathrm{mm}; \quad h(0) = \alpha h(l); \quad h(l) = 1\,\mathrm{mm}; \quad E = 10^5\,\mathrm{MPa}; \quad G = 4\cdot 10^4\,\mathrm{MPa} \tag{31}
$$

where α is the ratio between the maximum and the minimum cross-section sizes.

4.3.1. Beam behavior for vanishing taper slope

To evaluate the non-prismatic beam behavior for vanishing taper slope, we consider two cases:

1. a cantilever with an horizontal center-line i.e., $c(x) = 0$ where all the cross-sections are symmetric with respect to the beam longitudinal axis, denoted in the following as *symm*
2. a cantilever with an horizontal lower limit i.e., $h_l(x) = 0$ and $c(x) = (1-\alpha)\, h(l)\, \frac{x}{2l}$, denoted in the following as *unsym*

We investigate the model behavior when the parameter $\alpha \to 1$ i.e., when the beam becomes prismatic. Since it is not possible to evaluate analytically the displacement limit, we evaluate the maximum vertical displacement $v(l)$ varying α between 2 and $1 + 1 \cdot 10^{-9}$ mm.

The maximum vertical displacement for the Timoshenko beam solution, indicated in the following as v_{as} assume the following value:

$$v_{as} = \frac{1}{3}\frac{V(l)\, l^3}{E\frac{h^3}{12}} + \frac{6}{5}\frac{V(l)\, l}{Gh} = 0.0403\,\text{mm} \tag{32}$$

Figure 7(a) plots the variation of the maximum displacement as a function of the parameter α whereas

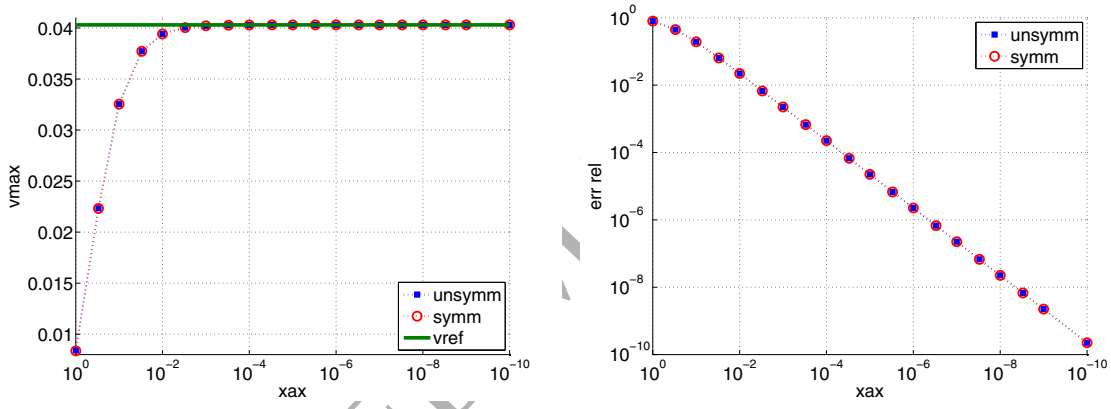

(a) Maximum vertical displacement $v(l)$ evaluated for different geometries and values of α.

(b) Asymptotic error e_{as} evaluated for different geometries and values of α.

Figure 7: Asymptotic behavior of a tapered cantilever loaded with a shear force $V(l) = 1\,\text{N}$ applied in the final cross-section.

Figure 7(b) plots the asymptotic error defined as

$$e_{as} = \frac{|v(l) - v_{as}|}{|v_{as}|} \tag{33}$$

We note that the effect of the non-horizontal center-line is negligible. Furthermore, the parameter α has a meaningful influence on the beam behavior for values greater than $1 + 1 \cdot 10^{-3}$. Performing calculations with standard double precision numbers, the solution starts to worsen for $\alpha < 1 + 1 \cdot 10^{-4}$ and calculations do not run for $a < 1 + 1 \cdot 10^{-7}$. Therefore, we use 50 digits precision numbers for the evaluation of the results reported in Figure 7.

Concluding, the model converges to the Timoshenko solution as expected. Furthermore, the analysis highlights some numerical problems in the model solution that fortunately occur for geometries without practical interest.

4.3.2. Effects of beam rotation

This subsection discusses the effect of a rotation of the global Cartesian coordinate system with respect to which we express the beam geometry. Due to the rotation θ of the Cartesian coordinate system, the

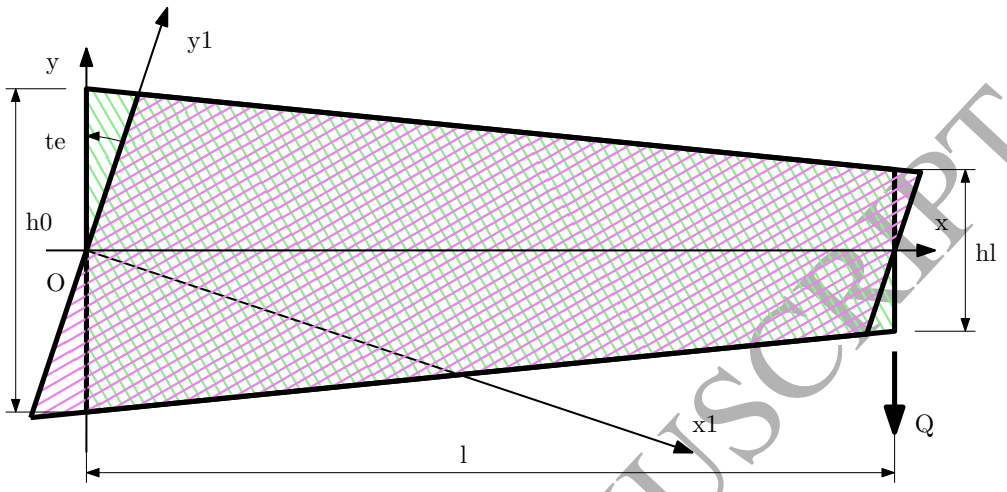

Figure 8: Symmetric tapered cantilever, geometry defintion through different Cartesian coordinate systems $l = 10\,\text{mm}$, $h\,(0) = \alpha h\,(l)$, $h\,(l) = 1\,\text{mm}$, $P = 1\,\text{N}$, $E = 10^5\,\text{MPa}$, and $G = 4 \cdot 10^4\,\text{MPa}$.

cross-sections will not remain perpendicular to the beam center-line and the beam geometry will change as illustrated in Figure 8. Nevertheless, we expect that the magnitude and the direction of the displacements evaluated in the final cross-section will not change.

We define the displacement magnitude relative error e_s and the displacement direction error Δ_θ as follows:

$$e_s = \frac{\left|\sqrt{u^2\,(l) + v^2\,(l)} - v\,(l)|_{\theta=0}\right|}{v\,(l)|_{\theta=0}}; \quad \Delta_\theta = \left|\arctan\left(\frac{u}{v}\right) - \theta\right| \tag{34}$$

Figure 9(a) displays the relative error e_s evaluated for different values of θ and α. The error becomes more significant for higher values of the rotation angle θ. Nevertheless, the error magnitude remains in a reasonable range for the most of practical applications. Figure 9(b) displays the displacement direction error Δ_θ for different values of θ and α. The results are reasonably accurate in predicting the right direction of displacement, at least in the considered cases.

4.4. Maximum displacement for symmetric, double-tapered beams

This section considers the double tapered beam loaded with a constant vertical load depicted in Figure 10. In particular, this geometry is of interest since it is often used to shape beams that support double pitched roofs.

According to several results reported in literature, we express the beam maximum displacement v_{max} as

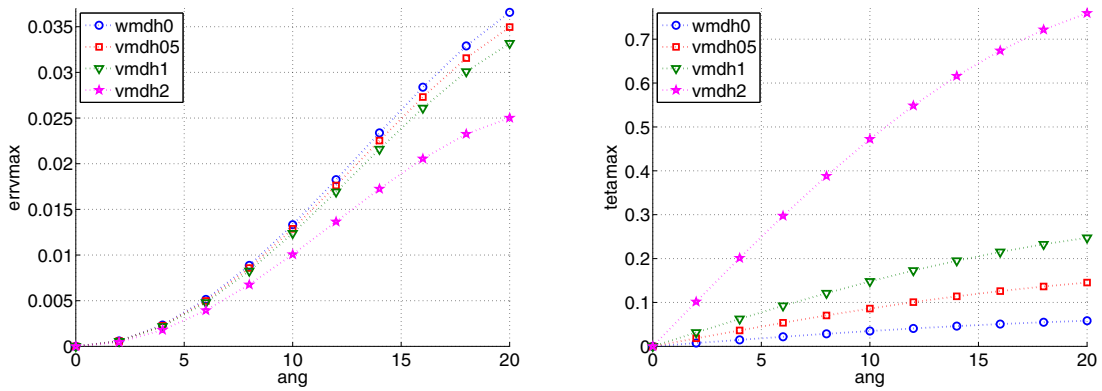

(a) Displacement magnitude relative error e_s evaluated for different rotations θ and values of α.

(b) Displacement direction error Δ_θ evaluated for different rotations θ and values of α.

Figure 9: Effects of the Cartesian coordinate system rotation on the behaviour of a tapered cantilever loaded with a shear force $P = 1\,\mathrm{N}$ applied in the final cross-section.

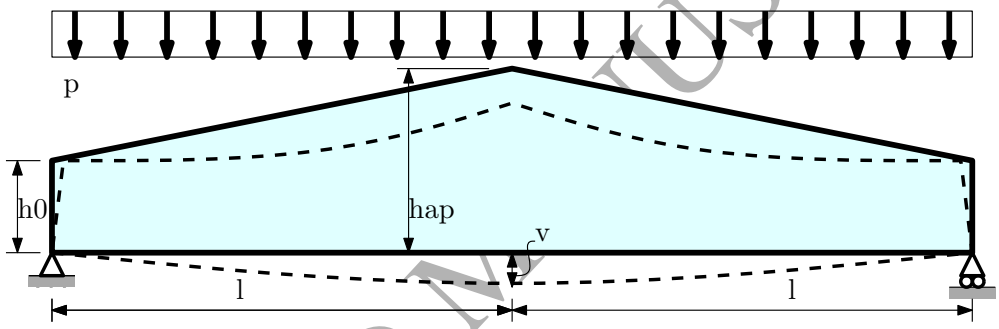

Figure 10: Double-tapered beam under constant and distributed vertical load p.

the sum of the bending v_E and the shear v_G contributions as follows:

$$v_{max} = v_E + v_G = -\frac{5}{384}\, k_E\, \frac{12}{h_0^3 b}\, \frac{pl^4}{E} - \frac{1}{8}\, k_G\, \frac{6}{5}\, \frac{pl^2}{G h_0 b} \tag{35}$$

Exploiting the beam symmetry, using both the homogeneous (29) and the particular (30) solutions, and imposing suitable boundary values (i.e., $u(0) = v(0) = M(0) = H(l/2) = V(l/2) = \varphi(l/2) = 0$) the coefficients k_E and k_G results defined as follows

$$\begin{aligned} k_E &= -\frac{6}{5}\, \frac{8\alpha^3 - 11\alpha^2 + 4\alpha - 1 - 2\alpha^2 \log(\alpha)\,(2\alpha + 1)}{\alpha^2\,(\alpha - 1)^4} \\ k_G &= -\frac{1}{2}\, \frac{29\alpha^3 - 40\alpha^2 + 15\alpha - 4 - 2\alpha^2 \log(\alpha)\,(8\alpha + 3)}{\alpha^2\,(\alpha - 1)^2} \end{aligned} \tag{36}$$

On the other hand, considering the model proposed by Rubin (1999), Schneider and Albert (2014) proposes the following expressions for the coefficients k_E and k_G:

$$k_E = \frac{1}{\alpha^3\left(0.15 + \frac{0.85}{\alpha}\right)}; \quad k_G = \frac{2}{1 + \alpha^{2/3}} \tag{37}$$

Finally, considering the Timoshenko prismatic beam equations, assuming only that cross-section area and inertia vary along the beam axis, Ozelton and Baird (2002) proposed the following expressions for the coefficients k_E and k_G:

$$\begin{aligned} k_E &= \frac{19.2}{(\alpha-1)^3}\left(2\frac{\alpha+2}{\alpha-1}\log\left(\frac{\alpha+1}{2}\right)+\frac{3}{\alpha+1}-\frac{2}{(\alpha+1)^2}-4\right) \\ k_G &= \frac{4}{\alpha-1}\left(\frac{\alpha+1}{\alpha-1}\log\left(\frac{\alpha+1}{2}\right)-1\right) \end{aligned} \tag{38}$$

Figure 11 reports the coefficients evaluated according to Equations (36), (37), and (38).

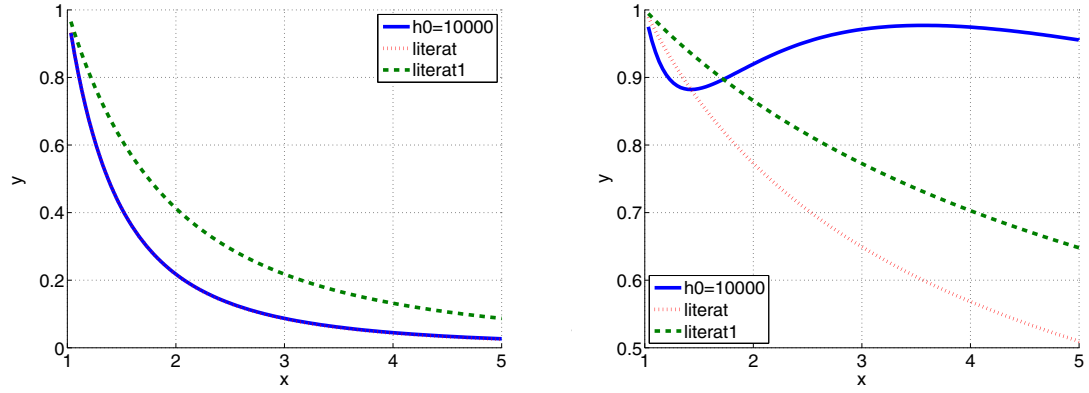

(a) Coefficient k_E evaluated for different values of α. (b) Coefficient k_G evaluated for different values of α

Figure 11: Coefficients k_E and k_G for the evaluation of the maximum displacement, evaluated with different methods.

All the functions reported in Figure 11 converge to 1 for $\alpha \to 1$. This is an expected behavior since if $\alpha = 1$ we are considering a prismatic beam and therefore no correction factors must be applied to Equation (35) in order to evaluate the beam maximum displacement. Figure 11(a) highlights that Equations (36) and (37) provide substantially identical evaluation of the coefficient k_E. On the other hand, with respect to the proposed model, Equation (38) overestimates the bending contribution of values that could exceed 100%. Figure 11(b) highlights that each model provides completely different evaluations of the coefficient k_G. Furthermore, with respect to the model derived in this paper, both the formulas proposed in literature underestimates the shear contribution of values that could exceed the 40%.

The adoption of Equations (36) in engineering practice needs additional considerations on material constitutive law and rigorous validations that lie outside this paper's aims. This specific aspect, as well as of other aspects of interest for practitioners, will be object of a further scientific paper.

5. Numerical examples

This section aims at providing further details about the obtained model capabilities. We consider two examples: (i) a tapered cantilever and (ii) an arch shaped beam. Both cases were already analyzed in

(Auricchio et al., 2015) considering a more refined model.

5.1. Tapered Beam

We consider the symmetric tapered beam illustrated in Figure 12 ($l = 10\,\text{mm}$, $h(0) = 1\,\text{mm}$, and $h(l) = 0.5\,\text{mm}$) and we assume $E = 10^5\,\text{MPa}$ and $G = 4 \cdot 10^4\,\text{MPa}$ as material parameters. Moreover, the beam is clamped in the initial cross-section $A(0)$ and a concentrated load $\boldsymbol{P} = [0, -1]\,\text{N}$ acts on the final cross-section $A(l)$.

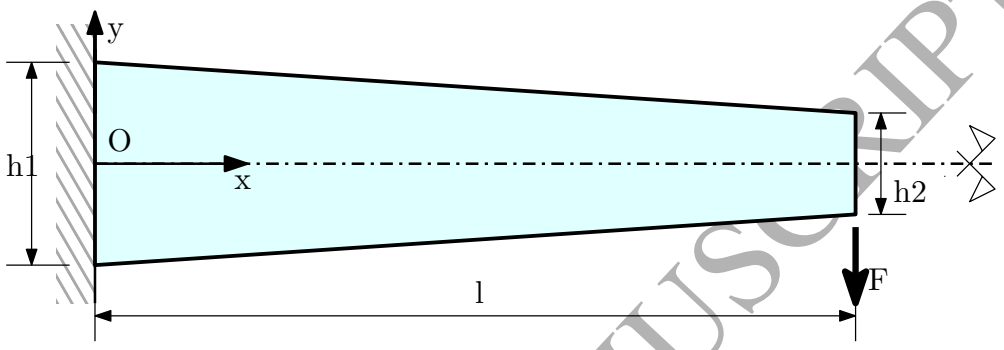

Figure 12: Symmetric tapered beam: $l = 10\,\text{mm}$, $h(0) = 1\,\text{mm}$, $h(l) = 0.5\,\text{mm}$, $P = 1\,\text{N}$, $E = 10^5\,\text{MPa}$, and $G = 4 \cdot 10^4\,\text{MPa}$.

Solving Equations (18), we obtain the following expressions for the generalized stresses

$$H(x) = 0; \quad M(x) = x - 10; \quad V(x) = 1 \tag{39}$$

Figure 13 depicts the distributions of the stresses σ_x and τ in the cross-section $A(0.5l)$. The label *mod* indicates the stress distribution obtained using Equations (19a) and (21), whereas the label *ref* indicates the 2D FE solution, computed using the commercial software ABAQUS (Simulia, 2011), considering the full 2D problem, and using a structured mesh of 7680×512 bilinear elements. Figure 13(b) allows to appreciate a

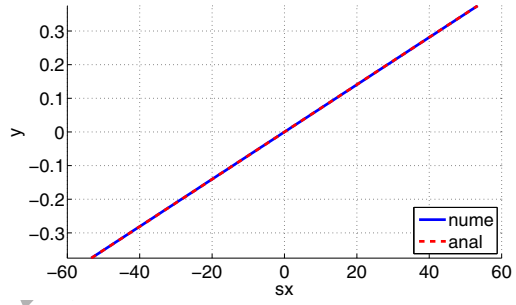

(a) Horizontal stress σ_x cross-section distribution.

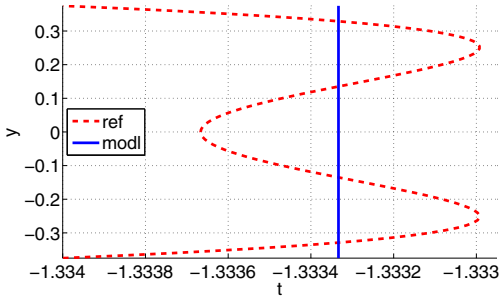

(b) Shear stress τ cross-section distribution.

Figure 13: Horizontal (Figure 13(a)) and shear (Figure 13(b)) stresses cross-section distributions, computed in the cross-section $A(0.5l)$ for a symmetric tapered beam with a vertical load $P = 1\,\text{N}$ applied in the final cross-section.

difference between the model and the reference solution, nevertheless the relative error magnitude is smaller than $1 \cdot 10^{-3}$.

Since $H(x) = 0$ therefore $\varepsilon_H H(x) = \chi_H H(x) = \gamma_H H(x) = 0$; moreover, since $c(x) = 0$ also $\varepsilon_M = \varepsilon_V = 0$. Figure 14 depicts the plots of the generalized deformations $\chi(x)$ and $\gamma(x)$. The curvature induced

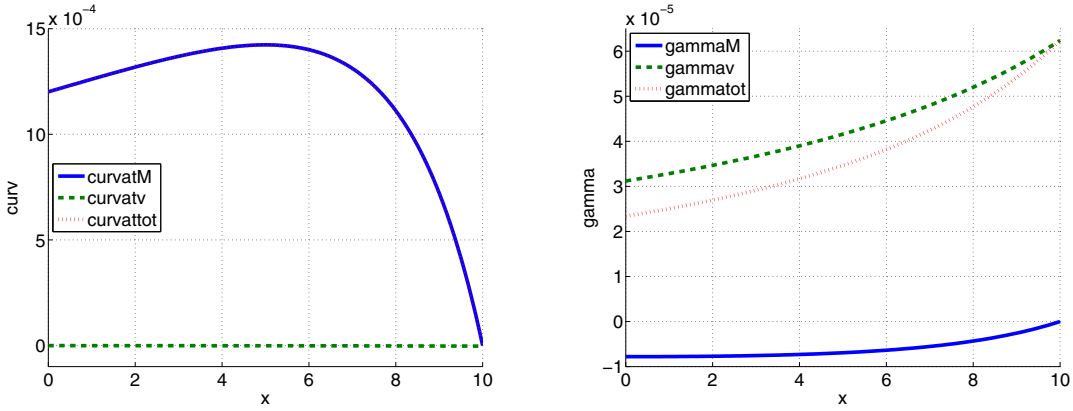

(a) Curvature $\chi(x)$ axial distribution.

(b) Shear deformation $\gamma(x)$ axial distribution.

Figure 14: Curvature (Figure 14(a)), and shear deformation (Figure 14(b)) axial distributions, evaluated for a tapered cantilever with a shear load $P = 1\,\mathrm{N}$ applied in the final cross-section.

by vertical forces $\chi_V V(x)$ has a negligible magnitude with respect to the curvature induced by resulting bending moment $\chi_M M(x)$. On the other hand both shear deformations $\gamma_M M(x)$ and $\gamma_V V(x)$ have the same order of magnitude and therefore both play a crucial role in determining the tapered beam's behavior.

Figure 15 reports the beam displacements $\varphi(x)$ and $v(x)$. Table 1 reports the maximum vertical dis-

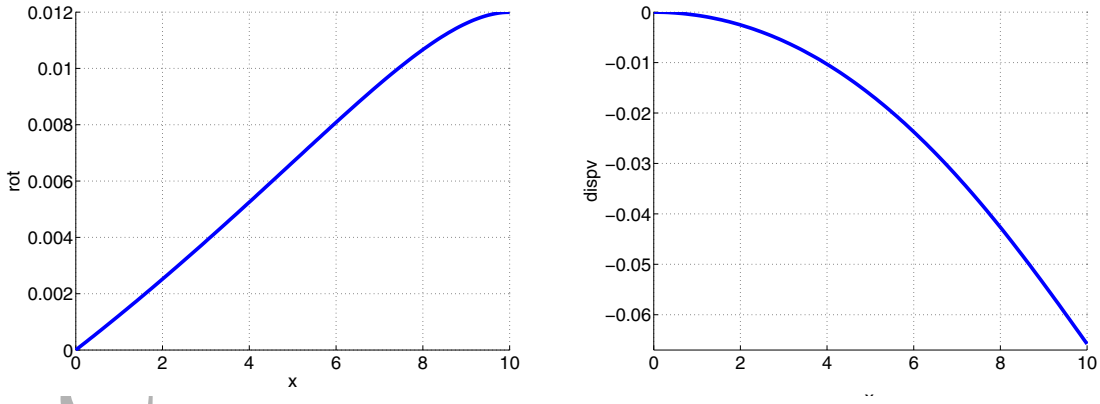

(a) Rotation $\varphi(x)$ axial distribution.

(b) Vertical displacement $v(x)$ axial distribution.

Figure 15: Rotation (Figure 15(a)) and vertical displacements (Figure 15(b)) axial distributions, evaluated for a tapered cantilever with a shear load $P = 1\,\mathrm{N}$ applied in the final cross-section.

placement evaluated with different models (i.e., the model proposed in this paper –indicated as Analytical model–, the model developed by Auricchio et al. (2015) –indicated as ABL–, and the FE analysis software ABAQUS –indicated as v_{ref}–). We note that all the models are accurate in predicting vertical displacement. Because it is more refined, ABL provides the most accurate prediction of vertical displacement whereas, be-

Beam model	$v\,(10)$ mm	$\frac{\lvert v-v_{ref}\rvert}{\lvert v_{ref}\rvert}$
Analytical model	-0.0657826	$1.064 \cdot 10^{-3}$
ABL	-0.0657294	$2.541 \cdot 10^{-4}$
2D solution (v_{ref})	-0.0657127	-

Table 1: Mean value of the vertical displacement evaluated on the final cross-section and obtained considering different models for a symmetric tapered cantilever with a vertical load $P = 1\,\mathrm{N}$ applied in the final cross-section.

ing less refined, the analytical model proposed in this paper is the less accurate. However, the analytical model shows a good accuracy, acceptable in most engineering applications.

5.2. Arch Shaped Beam

We now consider the arch shaped beam depicted in Figure 16. The beam center-line and cross-section height are defined as

$$c\,(x) := -\frac{1}{100}x^2 + \frac{1}{10}x; \quad h\,(x) := \frac{1}{50}x^2 - \frac{1}{5}x + \frac{3}{5} \tag{40}$$

Moreover, the beam is clamped in the initial cross-section $A\,(0)$ and loaded on the final cross-section $A\,(l)$ with a constant horizontal load distribution $\boldsymbol{t}|_{A(l)} = [1, 0, 0]^T$ N/mm.

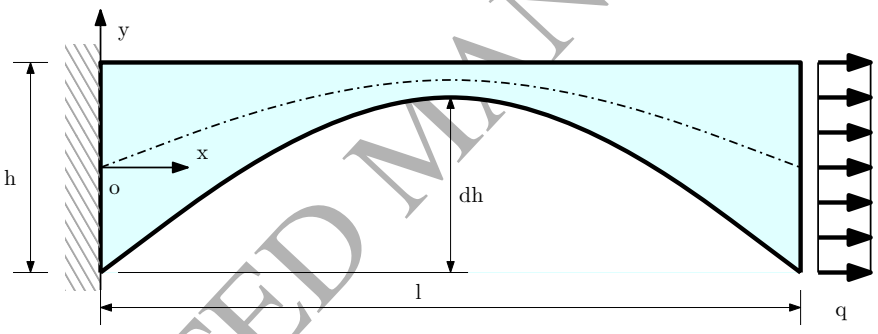

Figure 16: Arch shaped beam: $l = 10\,\mathrm{mm}$, $\Delta = 0.5\,\mathrm{mm}$, $h\,(l) = h\,(0) = 0.6\,\mathrm{mm}$, $q = 1\,\mathrm{N/mm}$, $E = 10^5\,\mathrm{MPa}$, and $G = 4 \cdot 10^4\,\mathrm{MPa}$.

Solving Equations (18), we obtain the following expressions for the generalized stresses

$$H\,(x) = \frac{3}{5}; \quad M\,(x) = \frac{3}{5} \cdot \left(-\frac{1}{100}x^2 + \frac{1}{10}x\right); \quad V\,(x) = 0 \tag{41}$$

Figure 17 depicts the cross-section distributions of the stresses σ_x and τ. The label *mod* indicates the stress distribution obtained using Equations (19a) and (21), whereas the label *ref* indicates the 2D ABAQUS solution, computed considering the full 2D problem and using a structured mesh of 10240×256 bilinear elements. In order to exclude boundary effects, we consider the cross-section $A\,(0.75l)$. We note the good agreement between the Analytical model and the 2D FE solution.

Since $V\,(x) = 0$ therefore we have $\varepsilon_V V\,(x) = \chi_V V\,(x) = \gamma_V V\,(x) = 0$. Figures 18(a), 18(c), and 18(d) depict the generalized deformation $\varepsilon_0\,(x)$, $\chi\,(x)$, and $\gamma\,(x)$ respectively. We note that the horizontal

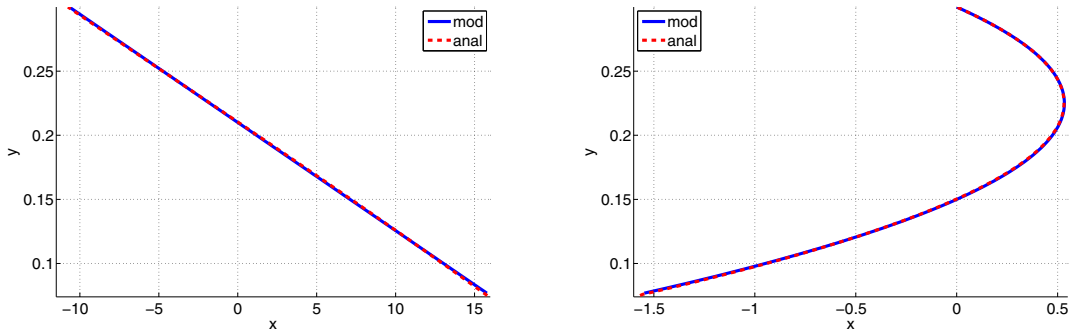

(a) Horizontal stress σ_x cross-section distribution.

(b) Shear stress τ cross-section distribution.

Figure 17: Horizontal (Figure 17(a)) and shear (Figure 17(b)) stresses cross-section distributions, computed in the cross-section $A\left(0.75l\right)$ for an arch shaped beam with an horizontal load $Q = 0.6\,\mathrm{N}$ applied in the final cross-section.

deformation induced by the bending moment $\varepsilon_M M\left(x\right)$ has negligible magnitude compared with the horizontal deformation induced by the resulting horizontal stress $\varepsilon_H H\left(x\right)$. Analogously, the curvature induced by resulting horizontal stress $\chi_H H\left(x\right)$ has a negligible magnitude with respect to the curvature induced by bending moment $\chi_M M\left(x\right)$. On the other hand, both the shear deformations induced by resulting horizontal stress $\gamma_H H\left(x\right)$ and bending moment $\gamma_M M\left(x\right)$ have non-vanishing magnitudes.

Figure 18(b) shows the horizontal elongation induced by center-line rotation $c'\left(x\right)\varphi$. This quantity is two order of magnitude bigger than the horizontal deformation $\varepsilon_0\left(x\right)$, and plays a central role in determining the horizontal displacements u.

Figure 19 reports the beam displacements $u\left(x\right)$, $\varphi\left(x\right)$, and $v\left(x\right)$.

Table 2 reports the maximum displacements $v\left(l\right)$ and $u\left(l\right)$ evaluated with different models. The reference

Beam model	$v\left(10\right)$ mm	$\frac{\lvert v-v_{ref}\rvert}{\lvert v_{ref}\rvert}$	$u\left(10\right)$ mm	$\frac{\lvert u-u_{ref}\rvert}{\lvert u_{ref}\rvert}$
Analytical model	0.222569	$5.979 \cdot 10^{-4}$	0.0109037	$5.598 \cdot 10^{-4}$
ABL	0.222434	$8.991 \cdot 10^{-6}$	0.0108971	$4.588 \cdot 10^{-5}$
2D solution (v_{ref}, u_{ref})	0.222436	-	0.0108976	-

Table 2: Mean value of the vertical and horizontal displacements computed on the final cross-section and obtained considering different models for an arch shaped beam with an horizontal load $Q = 0.6\,\mathrm{N}$ applied in the final cross-section.

solutions v_{ref} and u_{ref} are calculated using the ABAQUS software. The numerical results confirm that the analytical model is effective in predicting displacements despite it results less accurate than the model ABL.

6. Conclusions

The modeling of a generic non-prismatic planar beam proposed in this paper was done through 4 main steps

1. derivation of compatibility equations

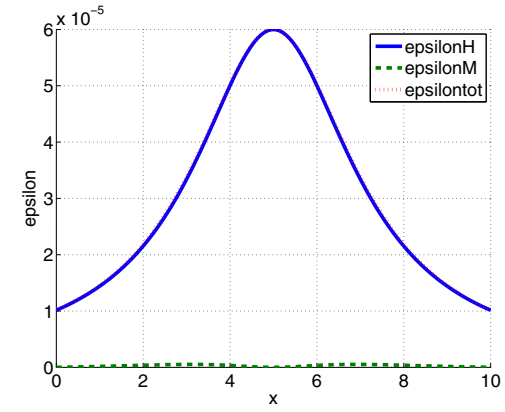

(a) Horizontal deformation $\varepsilon_0(x)$ axial distribution.

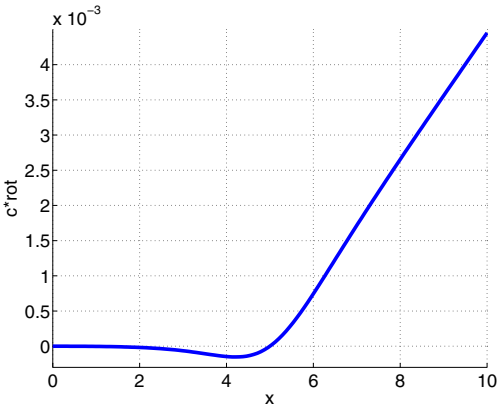

(b) Horizontal elongation induced by inclined center-line rotation $c'(x)\varphi$.

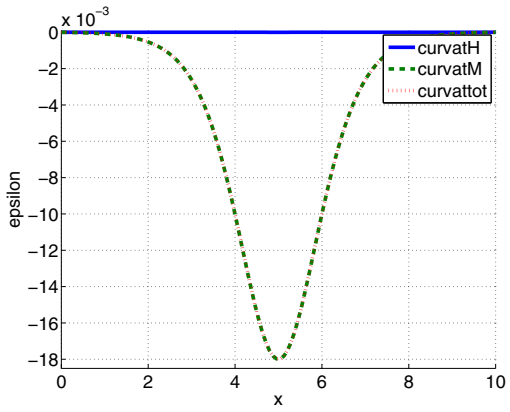

(c) Curvature $\chi(x)$ axial distribution.

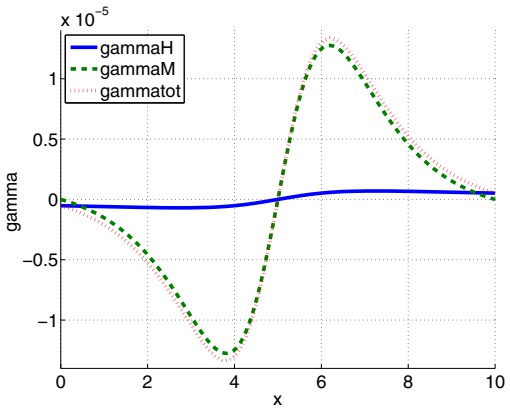

(d) Shear deformation $\gamma(x)$ axial distribution.

Figure 18: Horizontal (Figure 18(a)), curvature (Figure 18(c)), shear (Figure 18(d)) deformations, and horizontal elongation induced by inclined center-line rotation (Figure 18(b)) axial distributions evaluated for an arch shaped beam with an horizontal load $Q = 0.6\,\mathrm{N}$ applied in the final cross-section.

2. derivation of equilibrium equations
3. stress representation
4. derivation of simplified constitutive relations

In particular, compatibility and equilibrium equations are derived considering a global Cartesian coordinate system allowing the beam model to be expressed through simple ODEs. The stress representation takes accurately into account the boundary equilibrium of the body, and is crucial in determining the model effectiveness. The simplified constitutive relations need careful derivation and result in non-trivial equations.

The main conclusions highlighted by the derivation procedure and the discussion of practical examples can be resumed as follows.

- The shear distribution depends not only on vertical resulting stress but also on horizontal resulting stress and bending moment.

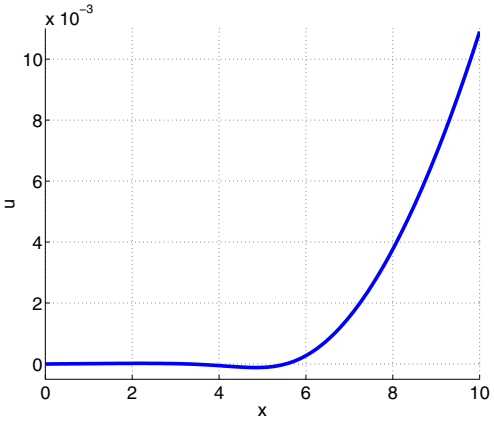

(a) Horizontal displacement $u\,(x)$.

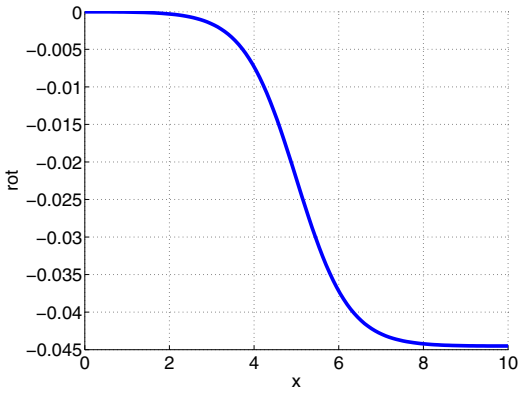

(b) Rotation $\varphi\,(x)$.

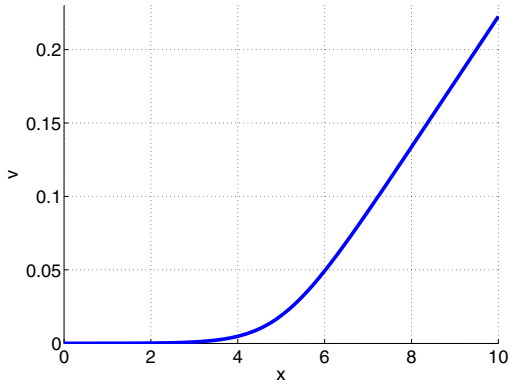

(c) Vertical displacement $v\,(x)$.

Figure 19: Horizontal (Figure 19(a)) and vertical (Figure 19(c)) displacements and rotation (Figure 19(b)) evaluated for an arch shaped beam with an horizontal load $Q = 0.6\,\mathrm{N}$ applied in the final cross-section.

- The complex geometry leads each generalized deformation to depend on all generalized stresses, in contrast with prismatic beams.
- The proposed model allows the evaluation of homogeneous and particular solutions in simple cases of practical interest.
- Example discussed in Section 5.2 highlights that non-prismatic beams could behave very differently than prismatic ones, even if they are slender and with very smooth cross-section variations.
- Numerical examples demonstrate that the proposed model gives effective and accurate results for complex geometries, so that the model is a promising tool for practitioners and researchers.

Further developments of the present work will include the application of the proposed model to more realistic cases in particular to the simplified modeling of wood structures, as well as the generalization of the proposed modeling procedure to 3D beams.

7. Acknowledgements

This work was partially funded by the Cariplo Foundation through the Projects iCardioCloud No. 2013-1179 and SICURA No. 2013-1351 and by the Foundation Banca del Monte di Lombardia – Progetto Professionalitá Ivano Benchi through the Project Enhancing Competences in Wooden Structure Design No. 1056.

References

Aminbaghai, M. and R. Binder (2006). Analytische Berechnung von Voutenstäben nach Theorie II. Ordnung unter Berücksichtigung der M- und Q- Verformungen. *Bautechnik 83*, 770–776.

Arunakirinathar, K. and B. D. Reddy (1992). Solution of the equations for curved rods with constant curvature and torsion. Technical report, Centre for research in computational and applied mechanics, University of Cape Town.

Arunakirinathar, K. and B. D. Reddy (1993). Mixed finite element methods for elastic rods orf arbitrary geometry. *Numerische Mathematik 64*, 13–43.

Atkin, E. H. (1938). Tapered beams: suggested solutions for some typical aircraft cases. *Aircraft Engineering 10*, 371–374.

Attarnejad, R., S. J. Semnani, and A. Shahaba (2010). Basic displacement functions for free vibration analysis of non-prismatic Timoshenko beams. *Finite Elements in Analysis and Design 46*, 916–929.

Auricchio, F., G. Balduzzi, and C. Lovadina (2015). The dimensional reduction approach for 2D non-prismatic beam modelling: a solution based on Hellinger-Reissner principle. *International Journal of Solids and Structures 15*, 264–276.

Balduzzi, G. (2013). *Beam Models: Variational Derivation, Analytical and Numerical Solutions*. Ph. D. thesis, Univeristà degli Studi di Pavia.

Balkaya, C. (2001). Behavior and modeling of nonprismatic members having T-sections. *Journal of Structural Engineering 8*, 940–946.

Balkaya, C. and E. Citipitioglu (1997). Discusson of the paper "stiffness formulation for nonprismatic beam elements" by Arture Tena-Colunga. *Journal of structural engineering 123*(12), 1694–1695.

Banerjee, J. R. and F. W. Williams (1985). Exact Bernoulli-Euler dynamic stiffness matrix for a range of tapered beams. *International Journal for Numerical Methods in Engineering 21*(12), 2289–2302.

Banerjee, J. R. and F. W. Williams (1986). Exact Bernoulli-Euler static stiffness matrix for a range of tapered beam-columns. *International Journal for Numerical Methods in Engineering 23*, 1615–1628.

Beltempo, A. (2013). Derivation of non-prismatic beam models by a mixed variational method. Master's thesis, Department of civil engineering and architecture – University of Pavia.

Beltempo, A., G. Balduzzi, G. Alfano, and F. Auricchio (2015). Analytical derivation of a general 2D non-prismatic beam model based on the Hellinger-Reissner principle. *Engineering Structures 101*, 88–98.

Boley, B. A. (1963). On the accuracy of the Bernoulli-Euler theory for beams of variable section. *Journal of Applied Mechanics 30*, 374–378.

Borri, M., G. L. Ghiringhelli, and T. Merlini (1992). Linear analysis of naturally curved and twisted anisotropic beams. *Composites Engineering 2*(5-7), 433–456.

Bruhns, O. T. (2003). *Advanced Mechanics of Solids*. Springer.

Capurso, M. (1971). *Lezioni di Scienza delle Costruzioni*. Pitagora Editrice Bologna.

Cicala, P. (1939). Sulle travi di altezza variabile. *Atti della Reale Accademia delle Scienze di Torino 74*, 392–402.

El-Mezaini, N., C. Balkaya, and E. Citipitioglu (1991). Analysis of frames with nonprismatic members. *Journal of Structural Engineering 117*, 1573–1592.

Franciosi, C. and M. Mecca (1998). Some finite elements for the static analysis of beams with varying cross section. *Computers and Structures 69*, 191–196.

Friedman, Z. and J. B. Kosmatka (1993). Exact stiffness matrix of a nonuniform beam - II bending of a Timoshenko beam. *Computers and Structures 49*(3), 545–555.

Fung, Y. C. and A. Kaplan (1952). Buckling of low arches or curved beams of small curvature. *National Advisory Commitee for Aeronautics 2840*, 1–75.

Gimena, L., F. Gimena, and P. Gonzaga (2008a). Structural analysis of a curved beam element defined in global coordinates. *Engineering Structures 30*, 3355–3364.

Gimena, F. N., P. Gonzaga, and L. Gimena (2008b). 3D-curved beam element with varying cross-sectional area under generalized loads. *Engineering Structures 30*, 404–411.

Gross, D., W. Hauger, J. Schröder, W. A. Wall, and N. Rajapakse (2012). Statics. In *Engineering Mechanics*. Springer.

Hodges, D. H., J. C. Ho, and W. Yu (2008). The effect of taper on section constants for in-plane deformation of an isotropic strip. *Journal of Mechanics of Materials and Structures 3*, 425–440.

Hodges, D. H., A. Rajagopal, J. C. Ho, and W. Yu (2010). Stress and strain recovery for the in-plane deformation of an isotropic tapered strip-beam. *Journal of Mechanics of Materials and Structures 5*, 963–975.

Kechter, G. E. and R. M.Gutkowski (1984). Double-tapered glulam beams: finite element analysis. *Journal of Structural Engineering 110*, 978–991.

Krahula, J. L. (1975). Shear formula for beams of variable cross section. *AIAA (American Institute of Aeronautics and Astronautics) journal 13*, 1390–1391.

Ozay, G. and A. Topcu (2000). Analysis of frames with non-prismatic members. *Canadian Journal of Civil Engineering 27*, 17–25.

Ozelton, E. C. and J. A. Baird (2002). *Timber designers' manual*. Blackwell Science Ltd.

Paglietti, A. and G. Carta (2007). La favola del taglio efficace nella teoria delle travi di altezza variabile. In *Atti del XVI Congresso dell'Associazione italiana di meccanica teorica e applicata, Brescia, 11-14 Settembre 2007*.

Paglietti, A. and G. Carta (2009). Remarks on the current theory of shear strength of variable depth beams. *The open civil engineering journal 3*, 28–33.

Popescu, B., D. H. Hodges, and C. E. S. Cesnik (2000). Obliqueness effects in asymptotic cross-sectional analysis of composite beams. *Computers and Structures 76*, 533–543.

Portland Cement Associations (1958). *Handbook of frame constants. Beam factor and moment coefficients for members of variable section*. Portland Cement Associations.

Rajagopal, A. and D. H. Hodges (2014). Asymptotic approach to oblique cross-sectional analysis of beams. *Journal of Applied Mechanics 81*(031015), 1–15.

Rajagopal, A., D. H. Hodges, and W. Yu (2012). Asymptotic beam theory for planar deformation of initially curved isotropic strips. *Thin-Walled Structures 50*, 106–115.

Rajasekaran, S. and S. Padmanabhan (1989). Equations of curved beams. *Journal of Engineering Mechanics 115*, 1094–1111.

Romano, F. (1996). Deflections of Timoshenko beam with varying cross-section. *International Journal of Mechanical Sciences 38*(8-9), 1017–1035.

Rubin, H. (1999). Analytische Berechnung von Stäben mit linear veränderlicher Höhe unter Berücksichtigung von M-, Q- und N- Verformungen. *Stahlbau 68*, 112–119.

Sapountzakis, E. J. and D. G. Panagos (2008). Shear deformation effect in non-linear analysis of composite beams of variable cross section. *International Journal of Non-Linear Mechanics 43*, 660–682.

Schneider, K. and A. Albert (2014). *Bautabellen für Ingenieure: mit Berechnungshinweisen und Beispielen*. Bundesanzeiger Verlag GmbH.

Shooshtari, A. and R. Khajavi (2010). An efficent procedure to find shape functions and stiffness matrices of nonprismatic Euler-Bernoulli and Timoshenko beam elements. *European Journal of Mechanics, A/solids 29*, 826–836.

Simulia (2011). *ABAQUS User's and theory manuals - Release 6.11*. Providence, RI, USA.: Simulia.

Tena-Colunga, A. (1996). Stiffness formulation for nonprismatic beam elements. *Journal of Structural Engineering 122*, 1484–1489.

Timoshenko, S. (1955). Elementary theory and problems. In *Strength of materials*. Krieger publishing company.

Timoshenko, S. and J. N. Goodier (1951). *Theory of Elasticity* (Second ed.). McGraw-Hill.

Timoshenko, S. P. and D. H. Young (1965). *Theory of Structures*. McGraw-Hill.

Vogel, U. (1993). Berechnung von Bogentragwerken nach der elastizitätstheorie II: Ordnung. Chapter 3.5 in Stahlbau Handbuch für Studium und Praxis Band 1, Teil A. *Stahlbau-Verlagsgesellschaft mbH Köln 1*, 211–226.

Vu-Quoc, L. and P. Léger (1992). Efficient evaluation of the flexibility of tapered i-beams accounting for shear deformations. *International journal for numerical methods in engineering 33*(3), 553–566.

Yu, W., D. H. Hodges, V. Volovoi, and C. E. Cesnik (2002). On Timoshenko-like modeling of initially curved and twisted composite beams. *International Journal of Solids and Structures 39*, 5101–5121.